

Probing the anomalous $Z\gamma\gamma$ and $Z\gamma Z$ vertices in radiative Møller scattering at Next Linear Collider energies

R. Walsh* and A. J. Ramalho†

Instituto de Física, Universidade Federal do Rio de Janeiro, Caixa Postal 68528, Ilha do Fundão, 21945-970 Rio de Janeiro, RJ, Brazil
(Received 16 September 2001; revised manuscript received 27 November 2001; published 20 February 2002)

In this paper we analyze the effects of the anomalous gauge boson couplings of the $Z\gamma\gamma$ and $Z\gamma Z$ vertices in radiative Møller scattering ($e^-e^- \rightarrow e^-e^- \gamma$) at the Next Linear Collider (NLC). The 95% confidence level limits for these trilinear couplings are evaluated considering three different sets of the e^-e^- NLC parameters. We also present a brief discussion on the sensitivity of the NLC to the form factor scale Λ .

DOI: 10.1103/PhysRevD.65.055011

PACS number(s): 12.60.Cn, 12.15.Ji

I. INTRODUCTION

Despite the successful description of the phenomenology of the electroweak and strong interactions, many physicists do not consider the standard model a fully satisfactory theory of fundamental interactions, since it does not answer some important questions. Regarding the shortcomings of the standard model, great efforts have been made by experimental groups [1] in order to search for deviations from the standard model predictions as an indication of new physics. Several extended models allowing the existence of new particles and interactions have been proposed by theorists. The self-interactions of the electroweak gauge bosons, as an important and sensitive probe of the standard model, have been extensively discussed in the literature. These interactions are well determined by the non-Abelian $SU(2) \times U(1)$ gauge symmetry of the standard model. Despite the early stage of the present experimental status with respect to the vector gauge boson self-interactions, in particular those among neutral gauge bosons, one can establish experimental bounds [2] on the parameters of the anomalous interactions. The current experimental limits suggest that new nonstandard physics would be set in around an energy scale Λ well above the electroweak scale. As soon as the proposed high energy colliders start running, an improvement on the sensitivity of the experiments to nonstandard trilinear vertices is expected.

The study of more detailed aspects of physics demands machines that satisfy certain requirements. The next generation of linear colliders [Next Linear Collider (NLC)] can provide both better defined initial and final states and an excellent discovery potential. The original projects for such machines allowed only e^+e^- collisions. However, further studies indicated that the addition of e^-e^- [3,4], $e^- \gamma$ and $\gamma\gamma$ modes before constructing the whole apparatus would be simple, low cost and very important to the NLC program, since a new and very rich physics can be reached [3–5]. The present designs for the e^-e^- NLC predict different stages of operation, allowing the center-of-mass energy to vary from 0.5 TeV to 1.5 TeV and the integrated luminosity to reach 500 fb^{-1} per year [3]. The nonzero total lepton number

gives a particular and important feature to the e^-e^- experiments not found in the e^+e^- counterparts. Total lepton number conservation implies very small backgrounds at the e^-e^- colliders. This e^-e^- option can be very important in searching trilinear anomalous vertices of both charged [5] and neutral gauge bosons. In this paper we analyze the possible effects of the $Z\gamma\gamma$ and $Z\gamma Z$ vertices in radiative Møller scattering, $e^-e^- \rightarrow e^-e^- \gamma$, considering three sets of NLC parameters (center-of-mass energy and integrated luminosity):

$$\begin{aligned} \sqrt{s} &= 0.5 \text{ TeV and } \mathcal{L} = 50 \text{ fb}^{-1}; \\ \sqrt{s} &= 1.0 \text{ TeV and } \mathcal{L} = 200 \text{ fb}^{-1}; \\ \sqrt{s} &= 1.5 \text{ TeV and } \mathcal{L} = 500 \text{ fb}^{-1}. \end{aligned}$$

In each case we bound physical regions in which the anomalous couplings become valid at the 95% confidence level (C.L.). We consider the new physics energy scale to be $\Lambda = 1.5 \text{ TeV}$. These results complement those obtained in $Z\gamma$ production in e^+e^- or pp colliders. It should be noted that the NLC upgrades implies more restrictive bounds on the anomalous couplings. We also analyze the sensitivity of the collider to the form factor scale Λ regarding each of these energy-luminosity prospects.

II. THE ANOMALOUS $Z\gamma\gamma$ AND $Z\gamma Z$ VERTICES

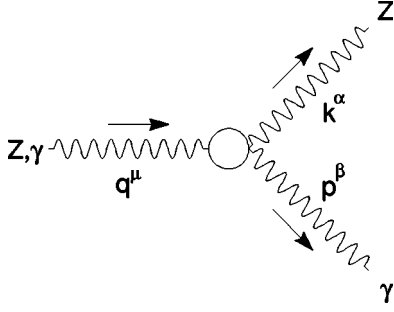
The most general trilinear $Z\gamma\gamma$ [6] and $Z\gamma Z$ [7] vertices in momentum space for an on-shell γ , consistent with Lorentz and gauge invariance, are given by

$$\begin{aligned} V_{Z\gamma\gamma}^{\alpha\beta\mu}(k,p,q) &= ie \frac{q^2}{M_Z^2} \left\{ h_1^\gamma (p^\mu g^{\alpha\beta} - p^\alpha g^{\mu\beta}) \right. \\ &+ \frac{h_2^\gamma}{M_Z^2} [q^\alpha (q \cdot p g^{\mu\beta} - p^\mu q^\beta)] + h_3^\gamma (\varepsilon^{\mu\alpha\beta\rho} p_\rho) \\ &\left. + \frac{h_4^\gamma}{M_Z^2} (\varepsilon^{\mu\beta\rho\sigma} q^\alpha q_\rho p_\sigma) \right\} \end{aligned} \quad (1)$$

*Electronic address: walsh@if.ufrj.br

†Electronic address: ramalho@if.ufrj.br

and


 FIG. 1. Anomalous $Z\gamma Z$ and $Z\gamma\gamma$ vertices.

$$\begin{aligned}
 V_{Z\gamma Z}^{\alpha\beta\mu}(k,p,q) = & ie \frac{q^2 - k^2}{M_Z^2} \left\{ h_1^Z (p^\mu g^{\alpha\beta} - p^\alpha g^{\mu\beta}) \right. \\
 & + \frac{h_2^Z}{M_Z^2} [q^\alpha (q \cdot p g^{\mu\beta} - p^\mu q^\beta) - k^\mu (k \cdot p g^{\alpha\beta} \\
 & - p^\alpha k^\beta)] + h_3^Z (\varepsilon^{\mu\alpha\beta\rho} p_\rho) \\
 & \left. + \frac{h_4^Z}{M_Z^2} (\varepsilon^{\mu\beta\rho\sigma} q^\alpha q_\rho p_\sigma - \varepsilon^{\alpha\beta\rho\sigma} k^\mu k_\rho p_\sigma) \right\}, \quad (2)
 \end{aligned}$$

respectively. Terms proportional to k^α or q^μ are neglected since the two virtual bosons couple to massless fermions.

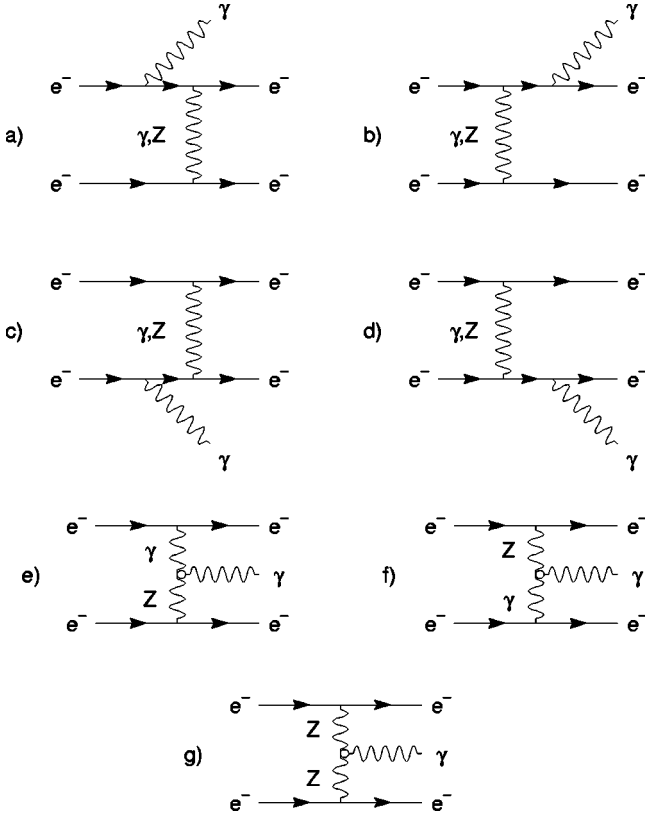


FIG. 2. Feynman diagrams for the radiative Møller scattering, $e^- e^- \rightarrow e^- e^- \gamma$. (a)–(d) correspond to the standard model diagrams, and diagrams (e)–(g) give the anomalous contributions.

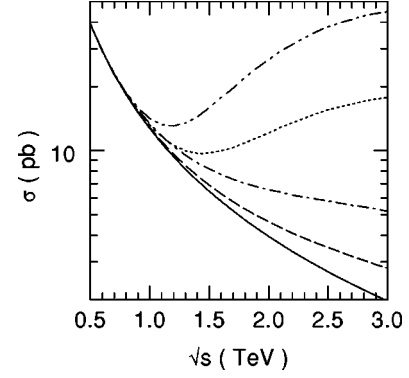


FIG. 3. Dependence of the total cross section on the center-of-mass energy \sqrt{s} . The solid curve represents the standard model prediction, while the dashed (dash-dotted) and dotted (dash-dot-dotted) curves receive the contribution from the anomalous couplings $h_{30}^Z (h_{30}^\gamma) = 0.4$ and $h_{40}^Z (h_{40}^\gamma) = 0.04$, respectively, for a form factor scale $\Lambda = 1.5$ TeV [same for $h_{10}^Z (h_{10}^\gamma) = 0.4$ and $h_{20}^Z (h_{20}^\gamma) = 0.04$, respectively].

Equations (1) and (2) are consistent with corresponding expressions obtained in Ref. [8]. The index assignments and momentum flow are given in Fig. 1. All anomalous couplings are C odd, h_1^V and h_2^V violate CP , whereas h_3^V and h_4^V are CP even, where $V = \gamma, Z$. In the standard model all eight couplings h_i^V vanish at the tree level. In order to satisfy unitarity,

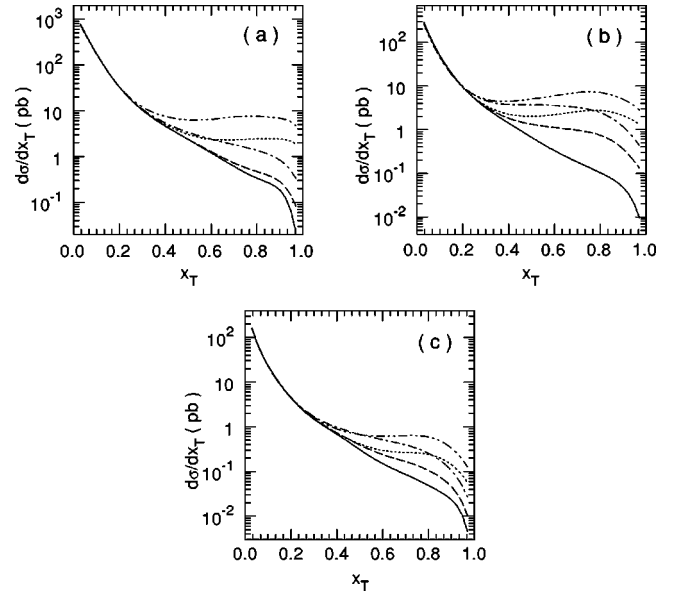


FIG. 4. Transverse momentum distributions for the photon at (a) $\sqrt{s} = 0.5$ TeV, (b) $\sqrt{s} = 1.0$ TeV and (c) $\sqrt{s} = 1.5$ TeV. The solid curves represent the standard model predictions. The dashed (dash-dotted) and dotted (dash-dot-dotted) curves correspond to the contribution of the anomalous couplings $h_{10}^Z (h_{10}^\gamma)$ and $h_{20}^Z (h_{20}^\gamma)$ respectively with the following numerical values: in graph (a), $h_{10}^V = 1.0$ and $h_{20}^V = 0.5$; in (b), $h_{10}^V = 0.5$ and $h_{20}^V = 0.05$; and in (c), $h_{10}^V = 0.1$ and $h_{20}^V = 0.005$, where $V = \gamma, Z$. An input scale $\Lambda = 1.5$ TeV is considered. For $h_{30}^V (h_{40}^V)$ instead of $h_{10}^V (h_{20}^V)$ the anomalous distributions behave essentially the same way.

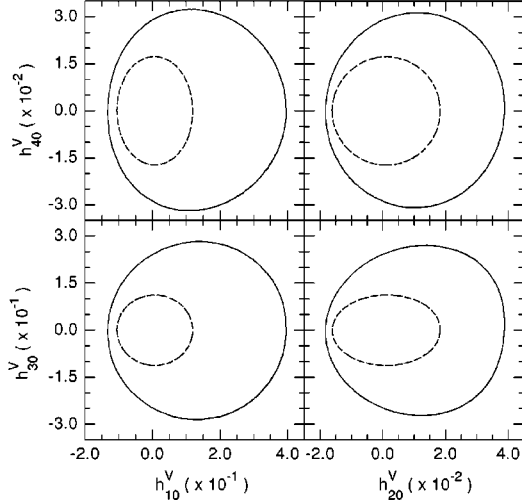
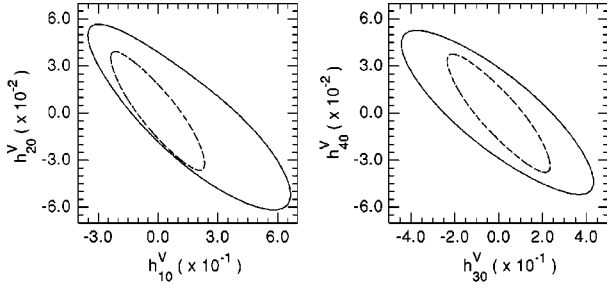


FIG. 5. 95% C.L. contours in the $h_{i0}^V-h_{j0}^V$ ($i,j=1\dots 4,i<j$) planes for $\sqrt{s}=0.5$ TeV and $\mathcal{L}=50$ fb $^{-1}$. The solid and dashed curves correspond to $V=Z$ and $V=\gamma$, respectively. The form factor scale is considered to be $\Lambda=1.5$ TeV.

we take the anomalous couplings as form factors $h_i^V(k^2, q^2)$, whose dependence on the invariants k^2 and q^2 must ensure Bose symmetry in each of the four terms of Eq. (2). Since these form factors must vanish at very large values of $|k^2|$ or $|q^2|$, we chose to express them in a dipole-like form [7],

$$h_i^V(q^2, k^2) = \frac{h_{i0}^V}{\left(1 - \frac{q^2 + k^2}{\Lambda^2}\right)^n}, \quad i=1\dots 4, \quad (3)$$

where h_{i0}^V are constants that represent the couplings values at low energies, $n=3$ for $h_{1,3}^V(k^2, q^2)$ and $n=4$ for $h_{2,4}^V(k^2, q^2)$. Λ is the energy scale around which nonstandard effects would become manifest.

III. CROSS SECTIONS AND LIMITS

The sensitivity to the anomalous couplings was tested by carrying out a Monte Carlo simulation of the process $e^-e^- \rightarrow e^-e^-\gamma$. The tree-level standard model Feynman diagrams are shown in Figs. 2(a)–2(d), whereas the anomalous $Z\gamma\gamma$ and $Z\gamma Z$ contributions are given by the diagrams (e)–(g). It is worthwhile to point out that in these anomalous graphs the two virtual boson lines are spacelike, differently of what hap-

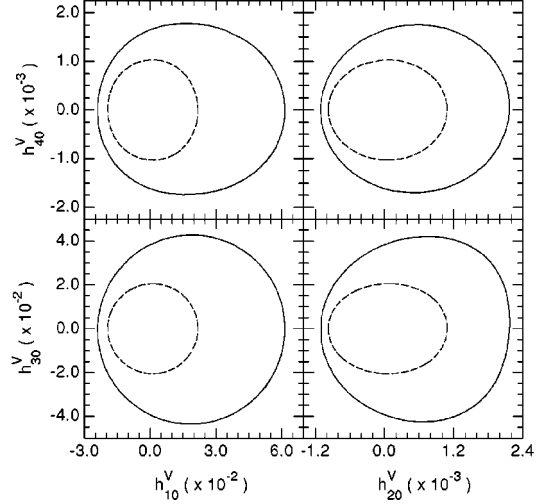
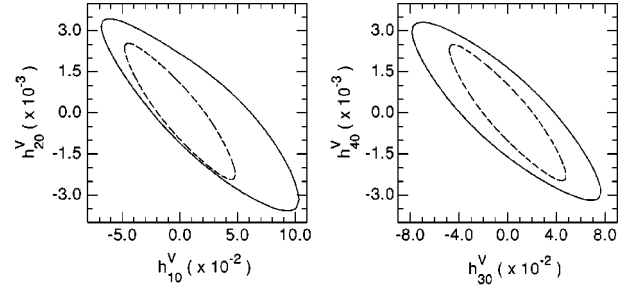


FIG. 6. Same as Fig. 5 but for $\sqrt{s}=1.0$ TeV and $\mathcal{L}=200$ fb $^{-1}$.

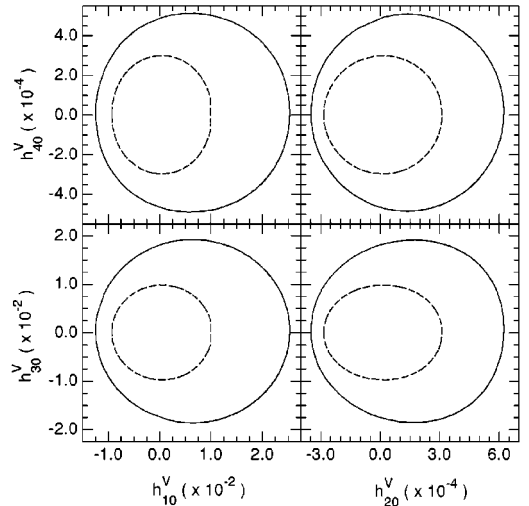
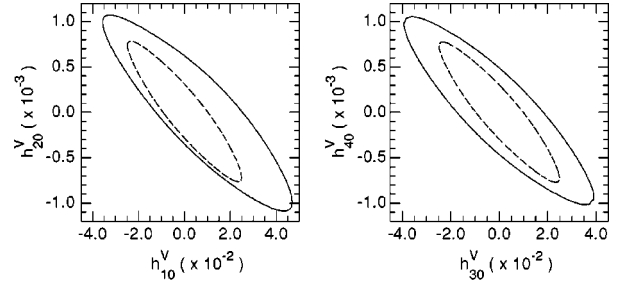


FIG. 7. Same as Fig. 5 but for $\sqrt{s}=1.5$ TeV and $\mathcal{L}=500$ fb $^{-1}$.

TABLE I. 95% C.L. constraints on correlated form factors for $\Lambda = 1.5$ TeV and for $\sqrt{s} = 0.5$ TeV (derived from Fig. 5).

Parameter	Negative limit	Positive limit	Correlation coefficient
h_{10}^Z	-3.6×10^{-1}	$+6.7 \times 10^{-1}$	-0.84
h_{20}^Z	-6.2×10^{-2}	$+5.7 \times 10^{-2}$	
h_{30}^Z	-4.5×10^{-1}	$+4.4 \times 10^{-1}$	-0.84
h_{40}^Z	-5.2×10^{-2}	$+5.3 \times 10^{-2}$	
h_{10}^Z	-1.4×10^{-1}	$+4.0 \times 10^{-1}$	$+5.1 \times 10^{-3}$
h_{30}^Z	-2.9×10^{-1}	$+2.9 \times 10^{-1}$	
h_{10}^Z	-1.4×10^{-1}	$+4.0 \times 10^{-1}$	$+5.6 \times 10^{-3}$
h_{40}^Z	-3.2×10^{-2}	$+3.3 \times 10^{-2}$	
h_{20}^Z	-1.9×10^{-2}	$+3.9 \times 10^{-2}$	$+2.7 \times 10^{-2}$
h_{30}^Z	-2.8×10^{-1}	$+2.8 \times 10^{-1}$	
h_{20}^Z	-1.9×10^{-2}	$+3.9 \times 10^{-2}$	$+1.4 \times 10^{-2}$
h_{40}^Z	-3.1×10^{-2}	$+3.2 \times 10^{-2}$	
h_{10}^γ	-2.4×10^{-1}	$+2.3 \times 10^{-1}$	-0.89
h_{20}^γ	-3.7×10^{-2}	$+3.9 \times 10^{-2}$	
h_{30}^γ	-2.4×10^{-1}	$+2.3 \times 10^{-1}$	-0.88
h_{40}^γ	-3.8×10^{-2}	$+3.8 \times 10^{-2}$	
h_{10}^γ	-1.1×10^{-1}	$+1.2 \times 10^{-1}$	-8.2×10^{-2}
h_{30}^γ	-1.1×10^{-1}	$+1.1 \times 10^{-1}$	
h_{10}^γ	-1.1×10^{-1}	$+1.2 \times 10^{-1}$	$+1.2 \times 10^{-2}$
h_{40}^γ	-1.7×10^{-2}	$+1.7 \times 10^{-2}$	
h_{20}^γ	-1.6×10^{-2}	$+1.8 \times 10^{-2}$	$+1.3 \times 10^{-2}$
h_{30}^γ	-1.1×10^{-1}	$+1.1 \times 10^{-1}$	
h_{20}^γ	-1.6×10^{-2}	$+1.8 \times 10^{-2}$	$+8.7 \times 10^{-4}$
h_{40}^γ	-1.7×10^{-2}	$+1.7 \times 10^{-2}$	

pens in $Z\gamma$ production in e^+e^- or pp colliders. The graphs corresponding to the exchanged final electrons are also considered in the calculation with the relative minus sign on account of the interchange of identical fermions, but they are not shown in Fig. 2. The amplitudes were evaluated numerically for convenience. Electrons in either the initial or final states are taken massless. The electroweak parameters we use are $M_Z = 91.187$ GeV, $\Gamma_Z = 2.49$ GeV, $\sin^2 \theta_W = 0.231$ and $\alpha(M_Z^2) = 1/128$. We imposed a 10 GeV cut on the energy of all final particles. We restricted polar angles, measured with respect to the beam direction, to be in the range $5^\circ < \theta_i < 175^\circ$, where $i = e, \gamma$ stand for the two final electrons and the photon. To avoid singularities we only account for events in which the photon and each of the electrons emerge with an angle of separation greater than 1° . Figure 3 shows the total cross section of the process we are considering as a function of the center-of-mass energy. The number of events per year predicted by the standard model is of the order of 10^6 for each set of NLC parameters. The four other curves in Fig. 3 account for the anomalous $Z\gamma\gamma$ and $Z\gamma Z$ contributions.

TABLE II. 95% C.L. constraints on correlated form factors for $\Lambda = 1.5$ TeV and for $\sqrt{s} = 1.0$ TeV (derived from Fig. 6).

Parameter	Negative limit	Positive limit	Correlation coefficient
h_{10}^Z	-6.9×10^{-2}	$+1.1 \times 10^{-1}$	-0.87
h_{20}^Z	-3.6×10^{-3}	$+3.5 \times 10^{-3}$	
h_{30}^Z	-7.9×10^{-2}	$+7.7 \times 10^{-2}$	-0.87
h_{40}^Z	-3.3×10^{-3}	$+3.4 \times 10^{-3}$	
h_{10}^Z	-2.5×10^{-2}	$+6.2 \times 10^{-2}$	-7.7×10^{-3}
h_{30}^Z	-4.4×10^{-2}	$+4.3 \times 10^{-2}$	
h_{10}^Z	-2.5×10^{-2}	$+6.2 \times 10^{-2}$	-5.1×10^{-3}
h_{40}^Z	-1.8×10^{-3}	$+2.5 \times 10^{-3}$	
h_{20}^Z	-1.2×10^{-3}	$+2.2 \times 10^{-3}$	$+2.4 \times 10^{-2}$
h_{30}^Z	-4.3×10^{-2}	$+4.3 \times 10^{-2}$	
h_{20}^Z	-1.2×10^{-3}	$+2.2 \times 10^{-3}$	$+2.1 \times 10^{-2}$
h_{40}^Z	-1.8×10^{-3}	$+1.8 \times 10^{-3}$	
h_{10}^γ	-4.8×10^{-2}	$+4.8 \times 10^{-2}$	-0.91
h_{20}^γ	-2.4×10^{-3}	$+2.6 \times 10^{-3}$	
h_{30}^γ	-4.8×10^{-2}	$+4.8 \times 10^{-2}$	-0.91
h_{40}^γ	-2.5×10^{-3}	$+2.5 \times 10^{-3}$	
h_{10}^γ	-1.9×10^{-2}	$+2.2 \times 10^{-2}$	-1.0×10^{-2}
h_{30}^γ	-2.1×10^{-2}	$+2.1 \times 10^{-2}$	
h_{10}^γ	-1.9×10^{-2}	$+2.2 \times 10^{-2}$	$+6.1 \times 10^{-3}$
h_{40}^γ	-1.0×10^{-3}	$+1.0 \times 10^{-3}$	
h_{20}^γ	-9.8×10^{-4}	$+1.1 \times 10^{-3}$	$+2.1 \times 10^{-2}$
h_{30}^γ	-2.1×10^{-2}	$+2.1 \times 10^{-2}$	
h_{20}^γ	-9.8×10^{-4}	$+1.1 \times 10^{-3}$	$+1.0 \times 10^{-2}$
h_{40}^γ	-1.0×10^{-3}	$+1.0 \times 10^{-3}$	

Their total event rates are comparable to the standard one up to $\sqrt{s} \sim 1.0$ TeV.

Among several kinematical distributions we found that the most sensitive to the anomalous couplings is the transverse momentum distribution of the final photon $d\sigma/dx_T$, where $x_T = 2p_T/\sqrt{s}$ is the scaled variable of the photon transverse momentum p_T . Distributions of this kind are shown in Fig. 4, both for the standard model and for anomalous couplings calculated with a form factor scale $\Lambda = 1.5$ TeV. Only high p_T photons receive contributions from the anomalous couplings. From Fig. 4 it can be inferred that the distribution is more sensitive to the h_2^V and h_4^V anomalous couplings than to h_1^V and h_3^V . Considering the $d\sigma/dx_T$ spectra we determined the form factors 95% confidence intervals by a χ^2 analysis. The range of x_T was divided into $n_B = 8$ bins and the χ^2 function defined as

$$\chi^2 = \sum_{i=1}^{n_B} \left(\frac{N_i^{SM} - N_i^{AN}}{\Delta N_i^{SM}} \right)^2, \quad (4)$$

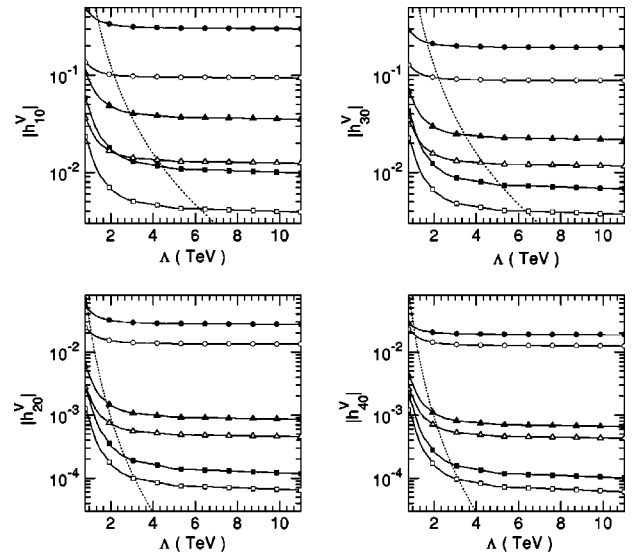
TABLE III. 95% C.L. constraints on correlated form factors for $\Lambda = 1.5$ TeV and for $\sqrt{s} = 1.5$ TeV (derived from Fig. 7).

Parameter	Negative limit	Positive limit	Correlation coefficient
h_{10}^Z	-3.6×10^{-2}	$+4.7 \times 10^{-2}$	-0.89
h_{20}^Z	-1.1×10^{-3}	$+1.1 \times 10^{-3}$	
h_{30}^Z	-4.0×10^{-2}	$+4.0 \times 10^{-2}$	-0.89
h_{40}^Z	-1.1×10^{-3}	$+1.1 \times 10^{-3}$	
h_{10}^γ	-1.3×10^{-2}	$+2.6 \times 10^{-2}$	-1.2×10^{-2}
h_{30}^γ	-1.9×10^{-2}	$+2.0 \times 10^{-2}$	
h_{10}^Z	-1.3×10^{-2}	$+2.6 \times 10^{-2}$	$+2.1 \times 10^{-2}$
h_{40}^Z	-5.0×10^{-4}	$+5.2 \times 10^{-4}$	
h_{20}^Z	-3.6×10^{-4}	$+6.3 \times 10^{-4}$	$+4.5 \times 10^{-3}$
h_{30}^Z	-1.9×10^{-2}	$+2.0 \times 10^{-2}$	
h_{20}^Z	-3.6×10^{-4}	$+6.3 \times 10^{-4}$	-2.0×10^{-2}
h_{40}^Z	-4.9×10^{-4}	$+5.2 \times 10^{-4}$	
h_{10}^γ	-2.5×10^{-2}	$+2.5 \times 10^{-2}$	-0.92
h_{20}^γ	-7.6×10^{-4}	$+7.9 \times 10^{-4}$	
h_{30}^γ	-2.5×10^{-2}	$+2.5 \times 10^{-2}$	-0.92
h_{40}^γ	-7.7×10^{-4}	$+7.8 \times 10^{-4}$	
h_{10}^γ	-9.3×10^{-3}	$+1.0 \times 10^{-2}$	-1.1×10^{-3}
h_{30}^γ	-9.8×10^{-3}	$+9.8 \times 10^{-3}$	
h_{10}^γ	-9.3×10^{-3}	$+1.0 \times 10^{-2}$	-5.4×10^{-3}
h_{40}^γ	-3.0×10^{-4}	$+3.0 \times 10^{-4}$	
h_{20}^γ	-2.9×10^{-4}	$+3.1 \times 10^{-4}$	$+6.7 \times 10^{-3}$
h_{30}^γ	-9.8×10^{-3}	$+9.8 \times 10^{-3}$	
h_{20}^γ	-2.9×10^{-4}	$+3.1 \times 10^{-4}$	$+1.5 \times 10^{-2}$
h_{40}^γ	-3.0×10^{-4}	$+3.0 \times 10^{-4}$	

where N_i^{SM} and N_i^{AN} are the number of events in the i^{th} bin predicted by the standard model and in the presence of anomalous couplings respectively, and the total error $\Delta N_i^{SM} = \sqrt{N_i^{SM} + (N_i^{SM} \delta)^2}$ is defined with the statistical and systematic errors added in quadrature. We considered a systematic error $\delta = 2\%$ for each measurement. We obtained the $h_{i0}^V - h_{j0}^V$; ($i, j = 1 \dots 4$, $i < j$) confidence regions whose 95% C.L. contours are displayed in Figs. 5, 6, and 7 for each set of NLC parameters. The form factor scale was taken to be $\Lambda = 1.5$ TeV. From Figs. 5, 6, and 7 we extracted the correlated bounds and correlation factors shown in Tables I, II, and III respectively. The sensitivity to the $Z\gamma\gamma$ and $Z\gamma Z$ couplings increases significantly with the center-of-mass energy. The correlations are very strong for pairs of form factors with same CP parity, whereas essentially no correlation is found for pairs of form factors with different CP parity, suggesting that CP -conserving effects may be disentangled from CP -violating ones. The $h_{i0}^\gamma - h_{j0}^Z$ ($i, j = 1 \dots 4$) contours, not displayed, obtained by combining the couplings from both anomalous vertices has shown essentially no cor-

 TABLE IV. 95% C.L. bounds on individual form factors for $\Lambda = 1.5$ TeV and for (a) $\sqrt{s} = 0.5$ TeV, (b) $\sqrt{s} = 1.0$ TeV, and (c) $\sqrt{s} = 1.5$ TeV.

	Parameter	Negative limit	Positive limit	
(a)	h_{10}^Z	-1.2×10^{-1}	$+3.7 \times 10^{-1}$	
	h_{20}^Z	-1.6×10^{-2}	$+3.6 \times 10^{-2}$	
	h_{30}^Z	-2.3×10^{-1}	$+2.2 \times 10^{-1}$	
	h_{40}^Z	-2.6×10^{-2}	$+2.7 \times 10^{-2}$	
	h_{10}^γ	-9.4×10^{-2}	$+1.1 \times 10^{-1}$	
	h_{20}^γ	-1.4×10^{-2}	$+1.7 \times 10^{-2}$	
	h_{30}^γ	-1.0×10^{-1}	$+1.0 \times 10^{-1}$	
	h_{40}^γ	-1.5×10^{-2}	$+1.5 \times 10^{-2}$	
	(b)	h_{10}^Z	-2.1×10^{-2}	$+5.8 \times 10^{-2}$
		h_{20}^Z	-9.6×10^{-4}	$+2.0 \times 10^{-3}$
h_{30}^Z		-3.6×10^{-2}	$+3.5 \times 10^{-2}$	
h_{40}^Z		-1.5×10^{-3}	$+1.5 \times 10^{-3}$	
h_{10}^γ		-1.7×10^{-2}	$+2.0 \times 10^{-2}$	
h_{20}^γ		-8.7×10^{-4}	$+9.8 \times 10^{-4}$	
h_{30}^γ		-1.8×10^{-2}	$+1.8 \times 10^{-2}$	
h_{40}^γ		-9.2×10^{-4}	$+9.2 \times 10^{-4}$	
(c)		h_{10}^Z	-1.1×10^{-2}	$+2.4 \times 10^{-2}$
		h_{20}^Z	-3.1×10^{-4}	$+5.8 \times 10^{-4}$
	h_{30}^Z	-1.6×10^{-2}	$+1.7 \times 10^{-2}$	
	h_{40}^Z	-4.2×10^{-4}	$+4.5 \times 10^{-4}$	
	h_{10}^γ	-8.3×10^{-3}	$+9.2 \times 10^{-3}$	
	h_{20}^γ	-2.5×10^{-4}	$+2.8 \times 10^{-4}$	
	h_{30}^γ	-8.7×10^{-3}	$+8.8 \times 10^{-3}$	
	h_{40}^γ	-2.7×10^{-4}	$+2.7 \times 10^{-4}$	


 FIG. 8. Dependence of the form factor bounds for $|h_{i0}^V|$ ($i = 1 \dots 4$) on the scale Λ . The solid (hollowed) symbols correspond to $V = \gamma$ (Z). The symbols representing the limits at $\sqrt{s} = 0.5$ TeV, $\sqrt{s} = 1.0$ TeV and $\sqrt{s} = 1.5$ TeV are circles, triangles and squares, respectively. The dotted lines display the respective partial wave unitarity bounds.

relation between them, i.e., effects arising from one anomalous vertex may be disentangled from the other one. This absence of correlation between h_{j0}^γ and h_{j0}^Z is due to the fact that the contribution to the amplitude of interference terms of the anomalous diagrams can be neglected. We also varied each form factor at a time, while all others were kept with their standard values. These one-degree-of-freedom 95% C.L. limits at each NLC energy appear in Table IV. To compare these limits with those already measured or theoretically estimated is not always straightforward, since the conventions adopted in the literature are not uniform. The bounds on anomalous couplings measured at CERN e^+e^- collider LEP and Fermilab Tevatron lie in the range $10^{-1} - 10^{-2}$ [2]. Some theoretical estimates for the CERN Large Hadron Collider (LHC) [1], very LHC (VLHC) [7] and NLC [9] point to limits of the order $10^{-3} - 10^{-4}$. Tables I–IV suggest that an e^-e^- version of the NLC could be competitive with other machines of next generation, as far as the determination of the structure of the anomalous $Z\gamma\gamma$ and $Z\gamma Z$ vertices is concerned.

The dependence of the bounds on the form factor scale Λ is displayed in Fig. 8. Whenever the absolute values of the positive and negative limits differed, only the largest of the two values was plotted. The corresponding partial wave unitarity bounds [6] are also illustrated in Fig. 8 for comparison. In general, the bounds on the form factors fall with increas-

ing values of Λ , reaching an asymptotic limit, which depends on the center-of-mass energy. From the experimental point of view, the NLC would be insensitive to any change in the form factor scale Λ beyond this asymptotic value. An increase in the center-of-mass energy allows that tighter limits be set on the form factors.

IV. CONCLUSIONS

We have discussed the possibility to search for the anomalous $Z\gamma\gamma$ and $Z\gamma Z$ vertices at the planned Next Linear Collider operating in the e^-e^- mode, at different energy-luminosity prospects. These trilinear vertices can be tested by means of the radiative Møller scattering which probes kinematical regions (two boson lines are spacelike) different from those of the usual $Z\gamma$ production in e^+e^- or pp colliders. The sensitivity of the process is enhanced at higher center-of-mass energies. Our results suggest that the e^-e^- mode, together with the planned upgrades of the NLC will become very important in the investigation of the structure of the $Z\gamma\gamma$ and $Z\gamma Z$ vertices.

ACKNOWLEDGMENTS

This work was partly supported by CNPq, FAPERJ and FINEP.

-
- [1] S. Haywood *et al.*, in *Proceedings of the Workshop on Standard Model Physics (and more) at the LHC*, CERN, Geneva, 2000, edited by G. Altarelli and M. L. Mangano (CERN Report No. 2000-004, Geneva, 2001), hep-ph/0003275, and references therein.
- [2] L3 Collaboration, M. Acciarri *et al.*, Phys. Lett. B **346**, 190 (1995); CDF Collaboration, F. Abe *et al.*, Phys. Rev. Lett. **74**, 1941 (1995); D0 Collaboration, S. Abachi *et al.*, *ibid.* **75**, 1028 (1995); DELPHI Collaboration, W. Adam *et al.*, Phys. Lett. B **380**, 471 (1996); D0 Collaboration, S. Abachi *et al.*, Phys. Rev. Lett. **78**, 3640 (1997); D0 Collaboration, B. Abbott *et al.*, Phys. Rev. D **57**, 3817 (1998); L3 Collaboration, M. Acciarri *et al.*, Phys. Lett. B **436**, 187 (1998); DELPHI Collaboration, P. Abreu *et al.*, *ibid.* **423**, 194 (1998); L3 Collaboration, M. Acciarri *et al.*, *ibid.* **489**, 55 (2000); OPAL Collaboration, G. Abbiendi *et al.*, Eur. Phys. J. C **17**, 553 (2000).
- [3] J. L. Feng, in *Proceedings of the 3rd International Workshop on Electron-Electron Interactions at TeV Energies*, Santa Cruz, CA, 1999 [Int. J. Mod. Phys. A **15**, 2355 (2000)], hep-ph/0002055.
- [4] C. A. Heusch, ITP Conference on Future High-Energy Colliders, Santa Barbara, CA, 1996, Santa Barbara 1996, Future High Energy Colliders, SLAC-PUB-7436, pp. 235–258.
- [5] D. Choudhury and F. Cuyper, Nucl. Phys. **B429**, 33 (1994).
- [6] U. Baur and E. L. Berger, Phys. Rev. D **47**, 4889 (1993).
- [7] Y. A. Coutinho, A. J. Ramalho, R. Walsh, and S. Wolck, Phys. Rev. D **64**, 115008 (2001).
- [8] G. J. Gounaris, J. Layssac, and F. M. Renard, Phys. Rev. D **62**, 073012 (2000).
- [9] R. Walsh and A. J. Ramalho, Phys. Rev. D **57**, 5908 (1998), and references therein.